

Instrumentation and biological applications of high-resolution frequency modulation atomic force microscopy in liquid

メタデータ	言語: English 出版者: 公開日: 2017-10-03 キーワード (Ja): キーワード (En): 作成者: Fukuma, Takeshi, 福間, 剛士 メールアドレス: 所属:
URL	https://doi.org/10.24517/00008297

This work is licensed under a Creative Commons Attribution-NonCommercial-ShareAlike 3.0 International License.



Instrumentation and Biological Applications of High-Resolution Frequency Modulation Atomic Force Microscopy in Liquid

Takeshi Fukuma^{1, 2, a}

¹Frontier Science Organization, Kanazawa University, Kakuma-machi, Kanazawa 920-1192, Japan

²PRESTO, Japan Science and Technology Agency, Honcho 4-1-8, Kawaguchi 332-0012, Japan

^afukuma@staff.kanazawa-u.ac.jp

Keywords: Frequency Modulation Atomic Force Microscopy, High-Resolution Imaging, Mica, Biological Membranes, Amyloid Fibrils.

Abstract. Frequency modulation atomic force microscopy (FM-AFM) has been a powerful tool for imaging atomic-scale structures and properties of various materials including metals, semiconductors, metal oxides, alkali halides and organic systems. Whilst the method has been used mainly in ultrahigh vacuum environments, recent progress in FM-AFM instrumentation made it possible to apply this technique also to investigations in liquid. This technological innovation opened up a variety of applications of FM-AFM in biology and electrochemistry. To date, the improved FM-AFM instrument and technique have been applied to investigations of several biological materials, providing novel information that has not been accessible with other imaging techniques. In this review, I will summarize the recent progress in FM-AFM instrumentation and biological applications in liquid.

Introduction

Frequency modulation atomic force microscopy (FM-AFM) was originally introduced by Albrecht *et al.* in 1991 for operating dynamic-mode atomic force microscopy (AFM) in ultrahigh vacuum (UHV) environments with a realistic imaging speed [1]. A UHV environment provides a high Q factor of the cantilever resonance hence high force sensitivity. It also allows us to investigate an atomically clean surface. In 1995, these factors, together with the advancements in instrumentation, made it possible to obtain true atomic resolution images by FM-AFM [2, 3]. In contrast to scanning tunneling microscopy (STM) [4], FM-AFM is applicable to investigations on insulating surfaces. In 1997, Bammerlin *et al.* presented the first true atomic resolution images of insulating surfaces [5]. In the same year, Fukui *et al.* presented the first true molecular resolution images of organic molecules [6].

Among the various applications explored after these pioneering works, here we focus on its applications to organic systems. From 1997 to 2000, main subject of this research area was to understand the imaging mechanism of organic molecules by FM-AFM. For this purpose, model organic systems that had been extensively studied by STM were imaged by FM-AFM [7-13]. The formation mechanism of the obtained molecular-scale contrasts was discussed in relation to the operation principle of FM-AFM. From 2000, the growing attention to molecular devices motivated researchers to investigate functional organic molecules such as self-assembled monolayers [14], organic semiconductors [15], organic ferroelectric materials [16], conductive polymers [17]. These studies made advancements in the understanding of imaging mechanism of FM-AFM and instrumentation required for stable high-resolution imaging of organic molecules.

Whilst the true molecular-resolution imaging technique of UHV-FM-AFM is becoming established, several research groups started to seek for the possibility of using FM-AFM in moderate vacuum, air or nitrogen atmosphere. There are several reasons for this trend. In contrast to reactive inorganic surfaces, organic molecules are relatively stable so that the use of UHV is not always essential. Molecular devices are expected to be used in air or at least in low vacuum condition, thus their structures and functions have to be investigated in such environments. The use of a UHV system

requires profound understanding of the vacuum system itself, which has limited the number of FM-AFM users especially in chemistry and biology. In 2002, Kobayashi *et al.* presented FM-AFM images obtained in air showing molecular rows of CuPc molecules [18]. In 2004, Sasahara *et al.* presented FM-AFM images obtained in N₂ atmosphere showing rows of TiO₂ surface [19]. Finally in 2004, Fukuma *et al.* presented the first true molecular resolution FM-AFM images obtained in air and moderate vacuum by imaging an alkanethiol monolayer and a polydiacetylene single crystal surface [20] using a home-built ultralow noise cantilever deflection sensor [21].

As for the liquid-environment applications of FM-AFM, Jarvis *et al.* [22] started to seek for the possibility at a very early stage, where majority of the research field focuses on the applications and instrumentation in UHV. In 2000, they utilized FM-AFM with a carbon nanotube tip for probing the oscillatory solvation force profiles at the solid/liquid interface [22]. They also pointed out the difficulty of operating FM-AFM in liquid because of the non-monotonous nature of frequency shift change with respect to the tip-sample distance and utilized dissipation signal for the distance regulation. In 2002, Kobayashi *et al.* presented FM-AFM image of Au(111) surface obtained in liquid using a home-built phase-locked loop (PLL) circuit [18]. Subsequently, Okajima and coworkers built a similar PLL circuit to operate FM-AFM in liquid and compared the amplitude and frequency changes near the tip-sample contact regime [23, 24]. The primary motivation for these studies was future applications to biological research. However, at this stage, the resolution of FM-AFM in liquid appeared to be on the order of ten nanometers or even worse, so that the technique did not seem to be very promising compared to alternative AFM techniques such as amplitude-modulation AFM (AM-AFM) and contact-mode AFM.

However, the situation was dramatically changed in 2005. Fukuma *et al.* developed a compact multi-environment FM-AFM that is capable of imaging molecules and atoms at subnanometer-resolution in vacuum, air and even in liquid [21]. True molecular-resolution images of polydiacetylene single crystal were obtained in vacuum, air and liquid with the same instrument. The first true atomic-resolution FM-AFM images were obtained by imaging mica in water [25]. This outstanding result stimulated subsequent research and motivated manufacturers of ambient and liquid environment AFMs to implement FM-AFM operation mode in their products. This dramatic improvement of FM-AFM performance in low Q environments was realized by three major improvements in the instrument and operating conditions. These key factors are discussed in detail in the following section. Subsequently, Fukuma *et al.* further improved the performance of the FM-AFM instrument [26] and applied it to the subnanometer-scale investigations on biological systems. These applications are reviewed in the third section of this article.

Instrumentation of Liquid-Environment FM-AFM

The major difficulty of FM-AFM operation in liquid has been ascribed to the Q factor of the cantilever resonance in liquid. Although there was no doubt that the low Q factor deteriorates the FM-AFM performance in liquid, no experimental or theoretical evidence was presented to conclude that the low Q factor is the only major limiting factor of FM-AFM performance in liquid. This was the major motivation for us to carry out quantitative and comprehensive noise analyses of FM-AFM performance from experimental and theoretical aspects. Consequently, we found the existence of other factors that has limited the noise performance of FM-AFM in low-Q environments. In the following section, I will summarize three major improvements that we made to overcome these limiting factors.

High Stiffness Cantilevers In liquid-environment AFM, it has been common to use relatively soft cantilevers. In contact-mode AFM, a cantilever with a spring constant (k) of less than 1 N/m is commonly used while a cantilever with $k = 0.1-3$ N/m is used in dynamic-mode AFM in liquid. On the contrary, a cantilever used in UHV for atomic-resolution imaging has much higher spring constant, i.e., 10-100 N/m typically. The root-mean-square (RMS) amplitude of thermal cantilever vibration is given by

$$\overline{z_B} = \sqrt{\frac{k_B T}{k}}, \quad (1)$$

where k_B and T are Boltzmann's constant and absolute temperature, respectively. For example, $\overline{z_B}$ values for $k = 0.4$ and 40 N/m are 100 pm and 10 pm, respectively. True molecular-resolution imaging by FM-AFM typically requires 10 pm vertical resolution. Therefore, in order to obtain true molecular-resolution, a cantilever with stiffness higher than 40 N/m has to be used. $\overline{z_B}$ can be reduced via a gentle contact of the tip with a sample such as in contact-mode AFM. However, it also hinders the precise control of the vertical tip position at atomic-scale contact/non-contact regimes. As this capability is essential for true atomic-resolution imaging as well as for atomic and molecular manipulations, it is desirable to use a stiff cantilever for such applications.

Small Oscillation Amplitude In 1999, Giessibl presented calculation results suggesting that the optimal cantilever oscillation amplitude (A) for high-resolution imaging by FM-AFM is on the order of the decay length of the force component to be detected [27]. For short-range forces that are responsible for the atomic-scale contrast formation, the length is typically less than 0.5 nm while the typical values for A used in FM-AFM had been larger than 5 nm. The validity of this argument was supported by the experimental results, showing subatomic-resolution contrasts of Si(111) surface [28]. The image was obtained with small oscillation amplitude (< 0.5 nm) and a stiff ($k = 1800$ N/m) cantilever. Although this particular experiment was performed in vacuum, the same argument should hold in air and liquid. By oscillating a cantilever with small amplitude, the tip front atom can experience short-range interaction for a longer time than it does with large amplitudes. As a result, the sensitivity to short-range interaction force is enhanced and that to long-range interaction force is reduced, leading to an improved spatial resolution.

In liquid-environment AFM, typical values for A had been 5 - 50 nm while Fukuma *et al.* utilized A of less than 0.5 nm for obtaining the first true atomic-resolution image in liquid [25]. In the case of vacuum environment, oscillating a cantilever with small amplitude requires the use of very stiff cantilever (e.g., 1800 N/m) for avoiding instabilities known as "jump-to-contact". In the case of liquid environment, the long-range forces such as van der Waals and electrostatic forces are greatly reduced by the existence of water molecules so that a cantilever with a spring constant of 40 N/m can be used without instabilities. This advantage partially compensates the large disadvantage of having a low Q factor in liquid. Namely, this is one of the reasons for that the spatial resolution obtained in liquid is comparable to that obtained in UHV in spite of the low Q factor.

Low Noise Deflection Sensor In FM-AFM, cantilever deflection signal is used not only for the frequency shift detection but also for generating a cantilever excitation signal. Therefore, a low noise deflection signal is required for the stable cantilever oscillation as well as for the high force sensitivity. This is particularly important when a cantilever is oscillated with small amplitude. In conventional liquid-environment AFM, power spectral density (PSD) of cantilever deflection signal arising from the deflection sensor (n_{zs}) is typically 100 - $1,000$ fm/ $\sqrt{\text{Hz}}$. On the other hand, the deflection sensor used for obtaining the first true atomic-resolution images in liquid has n_{zs} value of 17 fm/ $\sqrt{\text{Hz}}$ [21].

PSD of cantilever thermal Brownian motion n_{zB} is given by [1]

$$n_{zB} = \sqrt{\frac{2k_B T}{\pi f_0 k Q} \frac{1}{[1 - (f/f_0)^2]^2 + [f/(f_0 Q)]^2}}, \quad (2)$$

where Q is Q factor of the cantilever resonance. The total PSD of a cantilever deflection signal n_z is given by

$$n_z = \sqrt{n_{zs}^2 + n_{zB}^2}. \quad (3)$$

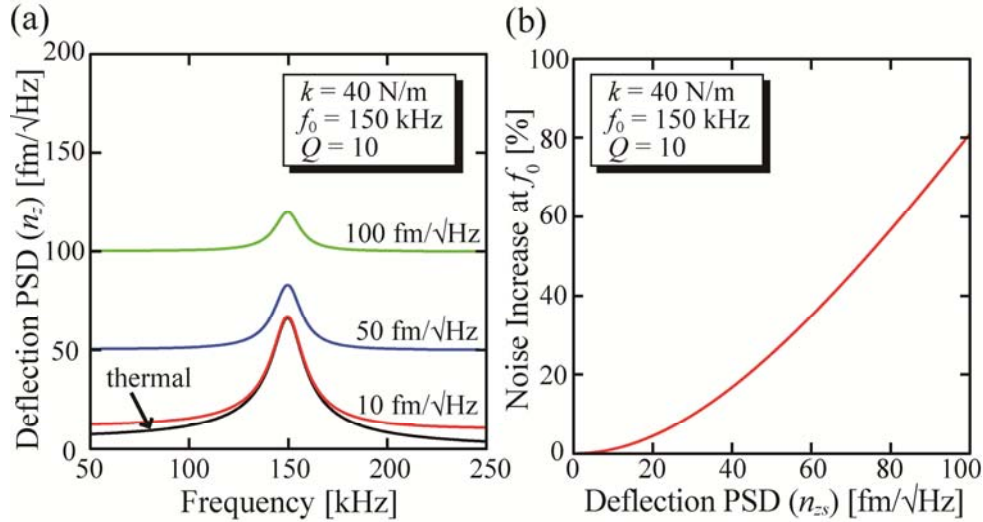


Fig. 1 (a) n_z values calculated with Eq. (2) and Eq. (3) for different n_{zs} . (b) The increase of deflection PSD at f_0 due to n_{zs} .

n_z values calculated with Eq. (2) and Eq. (3) are plotted in Fig. 1(a) for different n_{zs} values. With increasing n_{zs} from 10 to 100 $\text{fm}/\sqrt{\text{Hz}}$, the deviation from the thermal spectrum is dramatically increased. In dynamic-mode AFM, only the noise components in the frequency range from $f_0 - B$ to $f_0 + B$ (B : measurement bandwidth) influence the FM-AFM performance. As B is typically less than 1 kHz, the deflection noise in the frequency range is almost constant and given by

$$n_{zB}(f) = \sqrt{\frac{2k_B T Q}{\pi f_0 k}}. \quad (4)$$

From the ratio between n_z and n_{zB} at f_0 , we can estimate the increase of the noise as shown in Fig. 1(b). In order to suppress the noise increase to less than 10%, n_{zs} should be less than 30 $\text{fm}/\sqrt{\text{Hz}}$ for the typical cantilever used in liquid-environment FM-AFM. n_{zs} values for conventional AFMs are typically larger than 100 $\text{fm}/\sqrt{\text{Hz}}$, giving more than 80% increase of the noise in FM-AFM. Therefore, the noise performance in liquid is often limited not only by the low Q factor but also by the noise from the deflection sensor.

In 2005, Fukuma *et al.* presented a design of low noise optical beam deflection sensor having n_{zs} value of 17 $\text{fm}/\sqrt{\text{Hz}}$ in air and 40 $\text{fm}/\sqrt{\text{Hz}}$ in liquid [21] and obtained true atomic- and molecular-resolution images in liquid [25, 29]. The major improvement was brought about by the use of laser power modulation at 300 MHz for suppressing optical feedback and optical interference noises. Subsequently, in 2006 Fukuma *et al.* made a further improvement by refining the optical design and obtained 5.7 $\text{fm}/\sqrt{\text{Hz}}$ in air and 7.3 $\text{fm}/\sqrt{\text{Hz}}$ in liquid [26]. Now the design is further improved and the present sensor has n_{zs} value of 4.7 $\text{fm}/\sqrt{\text{Hz}}$ in liquid. Such an ultralow-noise deflection sensor allows to obtain the optimal noise performance limited only by the cantilever thermal vibration.

Biological Applications of Liquid-Environment FM-AFM

In 1993, Ohnesorge *et al.* reported the first true atomic-resolution images obtained in liquid using contact-mode AFM [30]. The technique has also been applied to high-resolution imaging of biological systems such as membrane proteins [31] and lipid bilayers [32]. Through these previous works, contact-mode AFM has been established as a high-resolution imaging tool at the solid/liquid interface. In 2005, Fukuma *et al.* introduced FM-AFM for obtaining true atomic-resolution images in liquid [25]. Since there was already an established method (i.e., contact-mode AFM), it was very important to demonstrate the advantages of using FM-AFM in biological studies. Compared to contact-mode AFM, FM-AFM has three major advantages in imaging applications, which include the precise control of vertical tip position at an atomic-scale contact/non-contact regime, high spatial

resolution, and capability of imaging isolated molecules. Following section summarizes the biological applications of FM-AFM, which highlights these three advantages.

Hydration Layers. In contact-mode AFM, a relatively soft cantilever ($k < 0.1$ N/m) is used especially in biological research. At atomic-scale contact/non-contact regimes, the tip experiences an attractive short-range interaction force that has large force gradient. Once the force gradient exceeds the spring constant of the cantilever, the tip jumps to contact with the surface, which is referred to as “jump-to-contact”. This instability hinders precise control of the vertical tip position at the near contact regimes. In the case of liquid-environment applications, it is possible to modify the interaction potential by adding salts [33]. However, this can limit the application range of contact-mode AFM in biology, where solution condition has considerable influence on the structure and dynamics of the molecules to be investigated. In FM-AFM, the use of stiff cantilever enables to detect the short-range interaction force without instability. In addition, in contact-mode AFM, a dc deflection of a cantilever is used as a feedback signal so that the dc drift of the deflection signal strongly influences the tip vertical position, i.e., loading forces during imaging. In FM-AFM, dc drift of a deflection signal hardly influences the frequency shift signal so that the vertical tip position is more stably controlled. Following example of FM-AFM application highlights this advantage.

Hydration layers on biological membranes are expected to have significant influence on the function of biological systems. If such hydration layers exist, they should alter the local interaction potential and present multiple energy barriers to the approaching nanoscale objects such as proteins and solvated ions. FM-AFM has a unique capability of probing local interaction force with a sharp tip. As the cross-section of the tip is comparable to the size of proteins and solvated ions, the interaction force detected by AFM should represent the interaction that approaching nanoscale objects would experience when they approach the membrane surface.

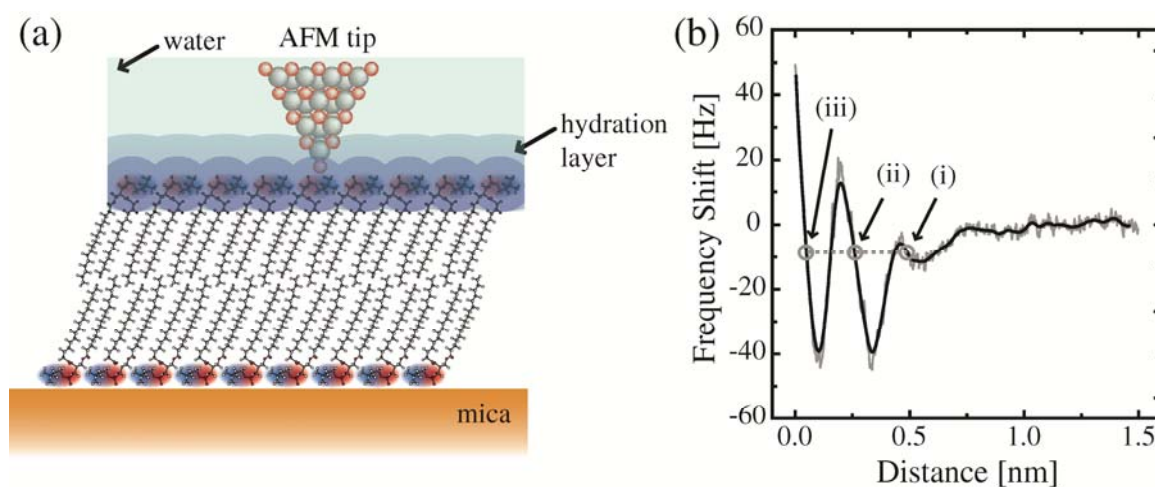


Fig. 2 (a) Schematic model of a DPPC bilayer formed on mica investigated by AFM in liquid. (b) Δf vs. distance curve measured on a DPPC bilayer in PBS solution, showing oscillatory profile with two peaks. The smoothed line (solid) is obtained by averaging the raw data (shaded) over the distance range of ± 0.02 nm from each data point. (Reused with permission from Fukuma *et al.* [34] Copyright 2007, Biophysical Society).

We employed FM-AFM to investigate the interface between a dipalmitoylphosphatidylcholine (DPPC) bilayer and phosphate buffer saline (PBS) solution as shown in Fig. 2(a). Figure 2(b) shows a frequency shift vs. distance curve measured on the DPPC bilayer in PBS solution [34]. The curve shows oscillatory profile with two peaks. The peak spacing is about 0.25 nm, which agrees with the diameter of a single water molecule. The result suggests that the oscillatory force profile originates from the water molecules confined between the tip and sample.

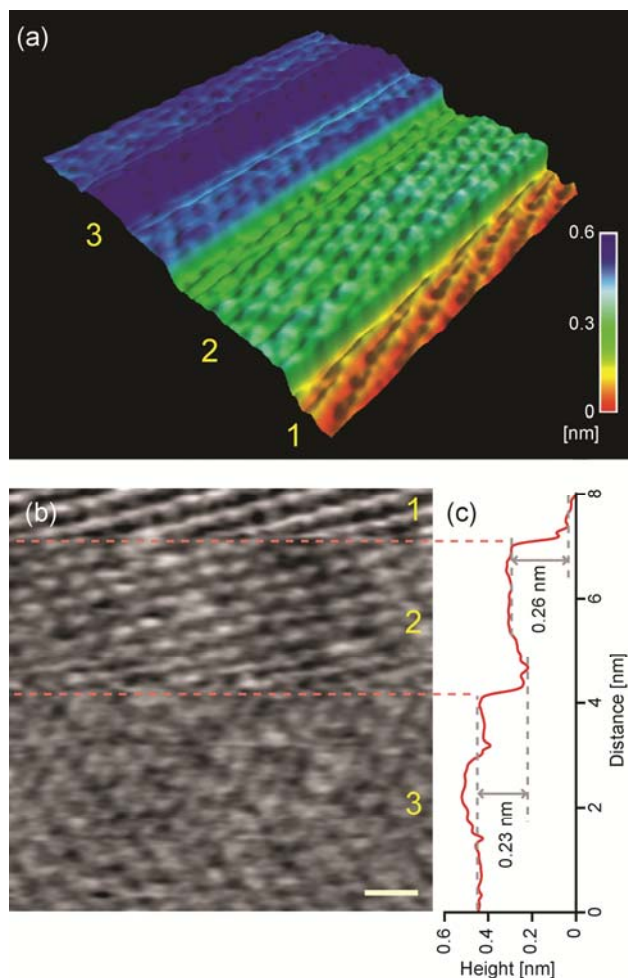


Fig. 3 (a) FM-AFM image of the DPPC bilayer in PBS solution showing spontaneous jumps during imaging. $8 \text{ nm} \times 8 \text{ nm}$, Tip velocity: 120 nm/s . Imaging speed: 85 s/frame . (b) Line-by-line flattened image of (a). Scale bar: 1 nm , Height range: 0.1 nm (black to white). Fast and slow scan directions: left to right and top to bottom. The regions indicated by the numbers 1, 2, and 3 correspond to the Terraces 1, 2, and 3 in (a). (c) Line-averaged height profile of (b) plotted along the slow scan direction. (Reused with permission from Fukuma *et al.* [34] Copyright 2007, Biophysical Society).

The excellent control of vertical tip position makes it possible to operate the tip-sample distance regulation even on the individual frequency shift branches indicated by the arrows in Fig. 2(b). An example of such imaging is shown in Fig. 3 [34]. An FM-AFM image obtained on the DPPC bilayer is shown in two different ways, namely, 3D view (Fig. 3(a)) and line-by-line flattened view (Fig. 3(b)). The image shows two discontinuous jumps during imaging. The tip is scanned from the bottom terrace (Terrace 1), where the tip is scanned directly on the lipid headgroups. The image shows corrugations corresponding to the individual lipid molecules. As the imaging progresses, the tip spontaneously jumped to the primary hydration layer (Terrace 2). The step height is about 0.26 nm , which corresponds to the scale of single water molecule. The image still shows corrugations of lipid molecules even on the primary hydration shell. The next step has a height of 0.23 nm . Although the molecular-scale corrugations become smaller, it is still visible in the image (Terrace 3). Such stable imaging on individual hydration layers highlights the excellent control of the vertical tip position in FM-AFM. The result also revealed the existence of stable hydration layers next to the lipid membrane with nanometer-scale lateral extension.

Lipid-Ion Networks. In contact-mode AFM, long-range and short-range interaction forces equally contribute to the static deflection of the cantilever. In FM-AFM, as the oscillation amplitude decreases, the sensitivity to short-range force is enhanced while that to long-range interaction force is reduced [27]. Consequently, the spatial resolution of FM-AFM is enhanced by reducing the

oscillation amplitude. In the following section, we present a biological application of FM-AFM, which demonstrates the benefit of such improved spatial resolution.

Physiological solution contains various metal cations, which have significant influence on structure and dynamics of biological membranes. For example, the addition of salts can trigger lipid bilayer phase separation [35-37] and vesicle aggregation processes [38, 39]. So far, a number of spectroscopy experiments have revealed that metal cations specifically interact with negatively charged moieties of the lipid headgroups [40–43]. These experiments, together with theoretical simulations [44], support the theory that individual ions may be interacting with multiple headgroups to form complex “lipid-ion networks” (Fig. 4(a)). This idea has been used to explain the observed influence of such ions in the enhanced mechanical strength of membranes [45] and the reduced mobility of the lipid molecules therein [46]. However, it has been a great challenge to experimentally access such lipid-ion networks due to the lack of a method for investigation of local lipid-ion interactions with Angstrom resolution. FM-AFM is capable of visualizing subnanometer-scale interaction potentials at the solid/liquid interface. Therefore, it should provide novel information that has not been obtained with alternative imaging techniques.

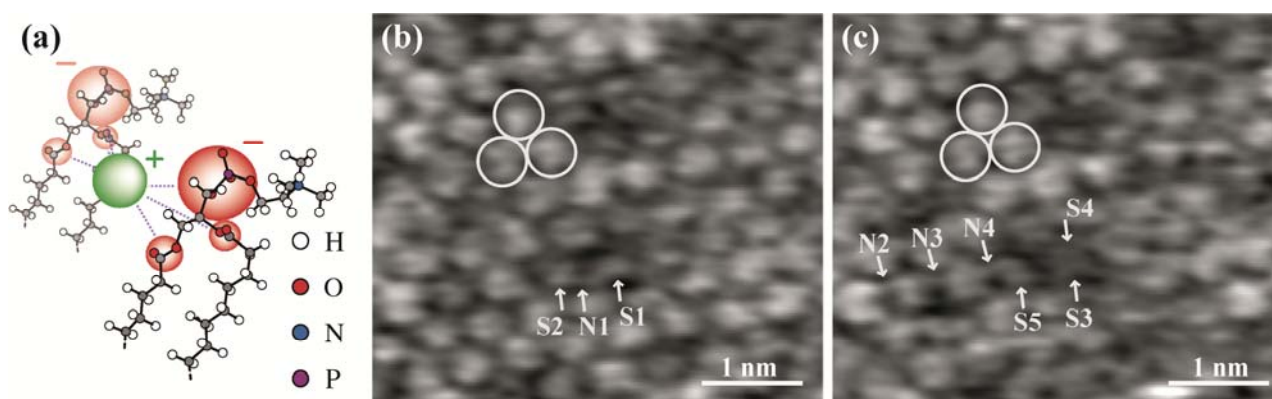


Fig. 4 (a) Schematic model of the lipid-ion complex formed at the lipid/water interface. (b) and (c) Sequential FM-AFM images of the same area of the DPPC bilayer in PBS solution. Height range: 0.1 nm. Tip velocity: 120 nm/s. Imaging speed: 85 s/image. (Reused with permission from Fukuma *et al.* [47] Copyright 2007, American Physical Society).

Figures 4(b) and 4(c) show sequential FM-AFM images of a DPPC bilayer in PBS solution [47]. The image was obtained at the interface between the lipid headgroups and the primary hydration layer. The surface consists of hexagonally arranged surface groups. Each surface group consists of two oval-shaped subunits separated by 0.1-0.2 nm. From the detailed analyses of AFM contrasts and previous studies using other techniques [42, 44, 48], it has been concluded that the image contrast represents averaged position of mobile ions interacting with the lipid headgroups. The two subunits represent the higher probability of existence of cations around the negatively charged two equivalent oxygen atoms in the phosphate group.

The sequential FM-AFM images shown in Fig. 4 reveal that some of the lipid-ion networks remain unchanged as indicated by the circles while the others show significant changes as indicated by the arrows. The lipid-ion network N1 in Fig. 4(b) disappears in Fig. 4(c) and networks N2-4 are formed. FM-AFM images visualize such formation and disappearance of lipid-ion networks at subnanometer-resolution. In addition, some of the lipid headgroups show structural changes upon formation or disappearance of lipid-ion networks. For example, subunit S1 does not have opposing subunit in Fig. 4(b). In Fig. 4(c), the same surface group shows two subunits S3 and S4. This has been attributed to the slight change of tilt angle of lipid headgroup. Such structural changes induced by the lipid-ion network formation suggest the existence of attractive interaction force mediated through the lipid-ion network. In fact, it has been known that the addition of metal cations to the solution increases the mechanical strength of the biological membranes [45]. The result presented here reveals the subnanometer-scale origin for such global effect of lipid-ion interaction.

Amyloid Fibrils. In contact-mode AFM, a tip is in contact with the surface during the tip scan. Thus, a relatively large lateral friction force is applied to the surface, which prevents imaging of isolated biomolecules weakly attached to a substrate. In FM-AFM, vertical motion of the cantilever dramatically reduces the lateral friction force, making it possible to image isolated biological molecules. In the following example, FM-AFM is used for imaging such isolated macromolecular assembly with subnanometer-resolution.

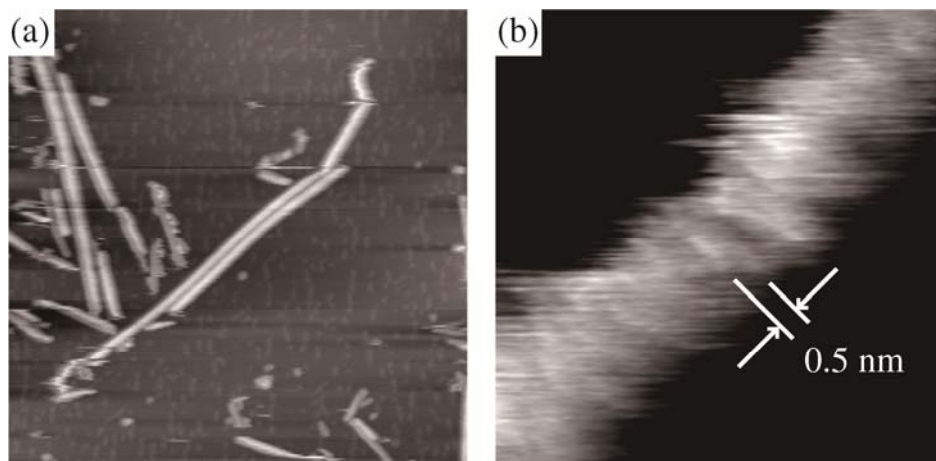


Fig. 5 FM-AFM images of IAPP fibrils on mica in PBS solution (a) $800 \text{ nm} \times 800 \text{ nm}$, $\Delta f = -55 \text{ Hz}$, tip velocity: $1 \mu\text{m/s}$. (b) $10 \text{ nm} \times 10 \text{ nm}$, $\Delta f = +50 \text{ Hz}$, tip velocity: 195 nm/s . (c) Schematic model of the β -strands. (Reused with permission from Fukuma *et al.* [49] Copyright 2008, Institute of Physics).

Amyloid fibrils are formed from various proteins which are normally soluble in aqueous solution. Under certain conditions, the precursor proteins misfold to form amyloid fibrils having an elongated structure as shown in Fig. 5(a). The fibrils are insoluble β -sheet structures that can form aggregates in tissues and organs, which are known as amyloid deposits. These deposits are found in a range of neurodegenerative diseases such as Alzheimer's, Parkinson's and Huntington's disease. Understanding the structure of amyloid fibrils is essential for elucidating the nucleation and kinetics of fibrillation in relation to the pathogenic pathway of amyloidoses.

Figures 5(a) and 5(b) show FM-AFM images of amyloid fibrils formed from the islet amyloid polypeptide (IAPP) deposited on mica in PBS solution. IAPP fibrils are associated with type II diabetes when deposited in pancreatic islets. The image shows fine stripe features perpendicular to the fibril axis. The distance between adjacent stripes is approximately 0.5 nm . A previous x-ray diffraction study suggested the existence of periodic structure along IAPP fibril axes with a spacing of 0.47 nm . The periodic structure was attributed to the alignment of the β -strands as this periodicity corresponds to hydrogen bond spacing between the β -strands, perpendicular to the fibril axis. The fine stripes observed in the FM-AFM image have comparable spacing aligned perpendicular to the fibril axis. Thus, the striped features are attributed to the β -strands of IAPP fibrils. This demonstrates the possibility of FM-AFM to visualize individual β -strands in real space in a physiologically-relevant liquid environment.

Summary

The theory and instrument of FM-AFM dramatically improved in the last ten years. The progress has made it possible to measure local interaction force with piconewton order sensitivity and to image subnanometer-scale structures at solid/liquid interfaces. Biological applications presented here demonstrate that FM-AFM is capable of visualizing interactions between biological molecules and surrounding physiological environment (i.e., water and ions) as well as structures of molecules

themselves. Such unique capability of FM-AFM should provide supplementary information that has not been accessible with other experimental techniques.

References

- [1] T. R. Albrecht, P. Grütter, D. Horne, D. Ruger, *J. Appl. Phys.* 69 (1991) 668.
- [2] F. J. Giessibl, *Science* 267 (1995) 68.
- [3] S. Kitamura, M. Iwatsuki, *Jpn. J. Appl. Phys. Part II* 34 (1995) L145.
- [4] G. Binnig, H. Rohrer, Ch. Gerber, and E. Weibel, *Phys. Rev. Lett.* 49 (1982) 57.
- [5] M. Bammerlin, R. Lüthi, E. Meyer, A. Baratoff, J. Lü, M. Guggisberg, C. Gerber, L. Howald, and H.-J. Güntherodt, *Probe Microscopy*, 1 (1997) 3.
- [6] K. Fukui, H. Onishi, and Y. Iwasawa, *Phys. Rev. Lett.* 79 (1997) 4202.
- [7] B. Gotsmann, C. Schmidt, C. Seidel, H. Fuchs, *Eur. Phys. J. B*, 4 (1998) 267.
- [8] K. Fukui, H. Onishi, Y. Iwasawa, *Appl. Surf. Sci.* 140 (1999) 259.
- [9] S. Kitamura, K. Suzuki, M. Iwatsuki, *Appl. Surf. Sci.* 140 (1999) 265.
- [10] K. Kobayashi, H. Yamada, T. Horiuchi, K. Matsushige, *Appl. Surf. Sci.* 140 (1999) 281.
- [11] K. Kobayashi, H. Yamada, T. Horiuchi, K. Matsushige, *Jpn. J. Appl. Phys.* 38 (1999) L1550.
- [12] T. Uchihashi, T. Okada, Y. Sugawara, K. Yokoyama, S. Morita, *Phys. Rev. B* 60 (1999) 8309.
- [13] T. Uchihashi, T. Ishida, M. Komiyama, M. Ashino, Y. Sugawara, W. Mizutani, K. Yokoyama, S. Morita, H. Tokumoto, and M. Ishikawa, *Appl. Surf. Sci.* 157 (2000) 244.
- [14] T. Fukuma, K. Kobayashi, T. Horiuchi, H. Yamada and K. Matsushige, *Appl. Phys. A* 72 (2001) S109-S112.
- [15] T. Fukuma, K. Kobayashi, H. Yamada and K. Matsushige, *J. Appl. Phys.* 95 (2004) 4742-4746.
- [16] T. Fukuma, K. Kobayashi, K. Noda, K. Ishida, T. Horiuchi, H. Yamada and K. Matsushige, *Surf. Sci.* 516 (2002) 103-108.
- [17] T. Ichii, H. Kawabata, T. Fukuma, K. Kobayashi, H. Yamada and K. Matsushige, *Nanotechnology* 16 (2005) S22-S26.
- [18] K. Kobayashi, H. Yamada, K. Matsushige, *Appl. Surf. Sci.* 188 (2002) 430.
- [19] A. Sasahara, S. Kitamura, H. Uetsuka, H. Onishi, *J. Phys. Chem. B* 108 (2004) 15735.
- [20] T. Fukuma, T. Ichii, K. Kobayashi, H. Yamada, K. Matsushige, *Appl. Phys. Lett.* 86 (2005) 034103.
- [21] T. Fukuma, M. Kimura, K. Kobayashi, K. Matsushige, H. Yamada, *Rev. Sci. Instrum.* 76 (2005) 053704.
- [22] S. P. Jarvis, T. Uchihashi, T. Ishida, H. Tokumoto, Y. Nakayama, *J. Phys. Chem. B* 104 (2000) 6091.
- [23] T. Okajima, H. Sekiguchi, H. Arakawa, A. Ikai, *Appl. Surf. Sci.* 210 (2003) 68.
- [24] H. Sekiguchi, T. Okajima, H. Arakawa, S. Maeda, A. Takashima, A. Ikai, 210 (2003) 61.
- [25] T. Fukuma, K. Kobayashi, K. Matsushige and H. Yamada, *Appl. Phys. Lett.* 87 (2005) 034101.
- [26] T. Fukuma and S. P. Jarvis, *Rev. Sci. Instrum.* 77 (2006) 043701.

- [27] F.J. Giessibl, H. Bielefeldt, S. Hembacher, J. Mannhart, *Appl. Surf. Sci.* 140 (1999) 352.
- [28] F. J. Giessibl, S. Hembacher, H. Bielefeldt, J. Mannhart, *Science* 289 (2000) 422.
- [29] T. Fukuma, K. Kobayashi, K. Matsushige and H. Yamada, *Appl. Phys. Lett.* 86 (2005) 193108.
- [30] F. Ohnesorge, G. Binnig, *Science* 260, 1451 (1993).
- [31] D. J. Müller, G. Büldt, A. Engel, *J. Mol. Biol.* 249 (1995) 239.
- [32] A. L. Weisenhorn, M. Egger, F. Ohnesorge, S. A. C. Gould, S.-P. Heyn, H. G. Hansma, R. L. Sinsheimer, H. E. Gaub, P. K. Hansma, *Langmuir* 7 (1991) 8.
- [33] D. J. Müller, D. Fotiadis, S. Scheuring, S. A. Müller, A. Engel, *Biophys. J.* 76 (1999) 1101.
- [34] T. Fukuma, M. J. Higgins, S. P. Jarvis, *Biophys. J.* 92 (2007) 3603.
- [35] M. Rappolt, G. Pabst, H. Amenitsch, P. Laggnier, *Coll. Surf. A* 183-185 (2001) 171.
- [36] M. Ross, C. Steinen, H.J. Galla, A. Janshoff, *Langmuir* 17 (2001) 2437.
- [37] J. T. Groves, S. G. Boxer, H. M. McConnell, *J. Phys. Chem. B* 104 (2000) 11409.
- [38] S. Ohki, N. Düzgüneş, K. Leonards, *Biochemistry* 21 (1982) 2127.
- [39] S. Ohki, K. Arnold, *Coll. Surf. B* 18 (2000) 83.
- [40] L. Herbette, C.A. Napolitano, R.V. McDaniel, *Biophys. J.* 46 (1984) 677.
- [41] C. Altenbach, J. Seelig, *Biochemistry* 23 (1984) 3913.
- [42] H. Binder, O. Zschörnig, *Chem. Phys. Lipids* 115 (2002) 39.
- [43] T. R. Hermann, A. R. Jayaweera, A. E. Shamoo, *Biochemistry*, 25 (1986) 5834.
- [44] M.L. Berkowitz, D.L. Bostick, S. Pandit, *Chem. Rev.* 106 (2006) 1527.
- [45] S. Garcia-Manyes, G. Oncins, F. Sanz, *Biophys. J.* 89 (2005) 1812.
- [46] R.A. Böckmann, A. Hac, T. Heimburg, H. Grubmüller, *Biophys. J.* 85 (2003) 1647.
- [47] T. Fukuma, M.J. Higgins, S.P. Jarvis, *Phys. Rev. Lett.* 98 (2007) 106101.
- [48] S. A. Pandit, D. Bostick, and M. L. Berkowitz, *Biophys. J.* 84 (2003) 3743.
- [49] T. Fukuma, A.S. Mostaert, S.P. Jarvis, *Nanotechnology* 19 (2007) 384010.